Transport Properties of Fluorite-Type $Ce_{0.8}Pr_{0.2}O_{2-\delta}$: Optimization via the Use of Cobalt Oxide Sintering Aid

Duncan P. Fagg,*[,†,‡] Susana García-Martin,[§] Vladislav V. Kharton,[||] and Jorge R. Frade[||]

Instituto de Cerámica y Vidrio, CSIC, Cantoblanco, Madrid-28049, Spain, Nanotechnology Research Division, Centre of Mechanical Technology and Automation (TEMA), University of Aveiro, 3810-193 Aveiro, Portugal, Departamento de Química Inorgánica, Facultad de Ciencias Químicas, Universidad Complutense, Madrid-28040, Spain, and Department of Ceramics and Glass Engineering, CICECO, University of Aveiro, 3810-193 Aveiro, Portugal

Received October 6, 2008. Revised Manuscript Received November 13, 2008

Dense $Ce_{0.8}Pr_{0.2}O_{2-\delta}$ ceramic membranes with submicron grain size can be formed at 1000 °C by minor additions of cobalt oxide. X-ray energy-dispersive spectroscopy shows the additive to be located in the grain boundary. Although a very fine grain interface is obtained for the composition containing 2 mol % cobalt oxide, pronounced grain boundary layers and Co-rich fringes are noted at 5 mol %. The cobalt oxide additions enhance electronic conductivity by around 2−3 times. For 2 mol % additions, no change to the level or nature of ionic conductivity is observed, whereas at 5 mol %, a depleted ionic conductivity is noted at lower temperatures. Coulombic titration studies show the bulk Pr oxidation state to be unaffected by the additions. Jointly, these results prove that the Co additions are not accommodated in the bulk material but instead form additive-rich grain boundary networks that are electronically conductive. Materials essentially free from oxygen surface exchange limitations are produced on addition of 2 mol % cobalt oxide, in contrast to that noted for 5 mol %. The combination of enhanced ambipolar conductivity and enhanced oxygen surface exchange kinetics boosts oxygen permeability in 2 mol % cobalt oxide doped $Ce_{0.8}Pr_{0.2}O_{2-\delta}$ to offer one of the highest levels of oxygen permeability reported to date for a single component mixed conducting fluorite material.

1. Introduction

In general, ceramic oxides with the fluorite structure have not shown promise as oxygen separation membranes because of low levels of ambipolar and electronic conductivities, despite the very high oxygen-ion diffusivities offered by doped ceria materials. As such, focus continues to rely heavily on the development of perovskite related materials for this application.[1,2] Recent studies on materials from the fluorite solid solution $Ce_{1-y}Pr_yO_{2-\delta}$ further support this trend showing uncompetitive levels of oxygen permeability for $Ce_{0.8}Pr_{0.2}O_{2-\delta}$ that are limited by both the level of electronic conductivity and oxygen surface exchange limitations.[3−6] The level of electronic conductivity in these materials could be most simply increased by increasing the dopant level of Pr.

However, this is prohibited in these materials due to the extent of the solid solution which is documented to exist only up to a Pr-content of $y = 0.3$.[3,7−9] Furthermore, this system suffers from high and non linear thermal expansion behavior and a large chemical expansion on reduction. These factors are exacerbated with increasing Pr content, preventing application due to expansion mismatch with other components and related failure. Several authors have suggested dopant regimes to control the thermal expansion behavior, but all efforts have been shown to impair transport properties.[4,6,9] As such, materials from the solid-solution $Ce_{1-y}Pr_yO_{2-\delta}$ are normally not competitive oxygen separation membranes, despite finding application as possible gas sensors, catalyst supports, and/or oxygen storage materials in automotive catalysts,[7,10−15] as a result of their ability to accommodate extensive deviations from stoichiometry with

* Corresponding author. Phone: 351-234-370263. Fax: 351-234-425300. E-mail: duncan@ua.pt.
† Instituto de Cerámica y Vidrio, CSIC.
‡ Centre of Mechanical Technology and Automation (TEMA), University of Aveiro.
§ Universidad Complutense.
|| CICECO, University of Aveiro.

(1) Bouwmeester, H. J. M.; Burggraaf, A. J. *Handbook on Solid State Electrochemistry*; Gellings, P. J., Bouwmeester, H. J. M., Eds.; CRC Press: New York, 1997; p 481.
(2) Thursfield, A.; Metcalfe, I. S. *J. Mater. Chem.* **2004**, *14*, 2475.
(3) Shuk, P.; Greenblatt, M. *Solid State Ionics* **1999**, *116*, 217.
(4) Fagg, D. P.; Kharton, V. V.; Shaula, A. L.; Marozau, I. P.; Frade, J. R. *Solid State Ionics* **2005**, *176*, 1723.
(5) Fagg, D. P.; Frade, J. R.; Kharton, V. V.; Marozau, I. P. *J. Solid State Chem.* **2006**, *179*, 1469.
(6) Fagg, D. P.; Marozau, I. P.; Shaula, A. L.; Kharton, V. V.; Frade, J. R. *J. Solid State Chem.* **2006**, *179*, 3347.
(7) Rossignol, S.; Descorme, C.; Kappenstein, C.; Duprez, D. *J. Mater. Chem.* **2001**, *11*, 2587.
(8) Nauer, M.; Ftikos, C.; Steele, B. C. H. *J. Eur. Ceram. Soc.* **1994**, *14*, 493.
(9) Ftikos, C.; Nauer, M.; Steele, B. C. H. *J. Eur. Ceram. Soc.* **1993**, *12*, 267.
(10) Logan, A. D.; Shelef, M. *J. Mater. Res.* **1994**, *9*, 468.
(11) Sinev, M. Y.; Graham, G. W.; Haack, L. P.; Shelef, M. *J. Mater. Res.* **1996**, *11*, 1960.
(12) Knauth, P.; Tuller, H. L. *J. Eur. Ceram. Soc.* **1999**, *19*, 831.
(13) Rajendran, M.; Mallick, K. K.; Bhattacharya, A. K. *J. Mater. Sci.* **1998**, *33*, 5001.
(14) Stefanik, T. S.; Tuller, H. L. *J. Eur. Ceram. Soc.* **2001**, *21*, 1967.
(15) Narula, C. K.; Haack, L. P.; Chun, W.; Jen, H. W.; Graham, G. W. *J. Phys. Chem. B* **1999**, *103*, 3634.

10.1021/cm802708a CCC: $40.75
Published on Web 12/22/2008

high rates of oxygen exchange and diffusion, with good stabilities in repeated redox cycles.

However, a recent communication showed that the minor addition of 2 mol % cobalt oxide as a sintering aid to $Ce_{0.8}Pr_{0.2}O_{2-\delta}$ can enhance electronic conductivity and effectively eradicate detrimental oxygen surface exchange limitations, to boost the level of oxygen permeability in these materials to levels that can compete with the more common perovskite separation membranes at intermediate temperatures.[16]

The idea behind this work stemmed from the observation of a significant enhancement of electronic conductivity in the material $Ce_{0.8}Gd_{0.2}O_{2-\delta}$ (CGO) by minor (2 mol %) additions of sintering aids,[17,18] and the observation that this enhancement of electronic conductivity dramatically improved oxygen reduction kinetics.[19] The current work now extends this work to assess the influence of Co concentration on transport and sintering properties and to assess the origin of the enhanced electronic conductivity both by microstructural studies and by columbic titration.

2. Experimental Section

Stoichiometric amounts of high-purity Pr_6O_{11} and $Ce(NO_3)_3 \cdot 6H_2O$ were dissolved in an aqueous solution of hot nitric acid. After being dried, the nitrate mixture was decomposed at 700 °C for 5 h. At this stage, single-phase powder of cubic defect fluorite $Ce_{0.8}Pr_{0.2}O_{2-\delta}$ is obtained.[16] The resultant powder was ball-milled in a nylon mill with zirconia balls. The cobalt oxide sintering aid was then added, at concentrations of 2 and 5 mol %, to the $Ce_{0.8}Pr_{0.2}O_{2-\delta}$ powder in the form of an aqueous solution of the nitrate followed by drying and further light milling in an agate pestle and mortar. Compositions with 0 mol % Co, 2 mol % Co, and 5 mol % Co-doped $Ce_{0.8}Pr_{0.2}O_{2-\delta}$ are hereafter labeled P2, P2C2, and P2C5, respectively. Pellets of the Co-doped and Co-free materials were uniaxially dry pressed at a pressure of 30 MPa followed by isostatic pressing at 200 MPa. Sintering behavior was studied on a Linseis dilatometer on rectangular green compacts approximately (2 mm × 3 mm × 8 mm) with a constant heating rate of 5 °C/min. Fresh disk-shaped samples of diameter approximately 20 mm were prepared for microstructural and electrical characterization. Co-free compositions were sintered at 1600 °C for 10 h, whereas Co-doped compositions were sintered at 1000 °C for 5 h. In both cases, the cooling rate was 2 °C/min.

Overall phase composition was determined by X-ray diffraction (XRD) using a Rigaku Geigerflex diffractometer (Cu Kα radiation; 5−80°, step 0.02, 6 s/step). Unit-cell parameters were determined using Materials Data Inc. Jade6 software, pseudo voight profile fit, and an external silicon standard for zero point correction.

X-ray energy-dispersive spectroscopy (XEDS) analyses were carried out with a scanning electron microscope JEOL 6400 working at 20 kV and with a transmission electron microscope JEM 3000F operating at 300 kV (double tilt ± 20°). For the SEM study, samples were polished and then thermally etched for 60 min at temperatures 100 K below that of the sintering temperature. Average grain sizes were calculated from SEM images (not shown) using an image processing program based on the intercept method. For transmission electron microscopy, the samples were ground in *n*-butyl alcohol and ultrasonically dispersed. A few drops of the resulting suspension were deposited in a carbon-coated grid. For ceramics with submicrometer grains, accurate determination of grain boundary composition by EDS is beyond the instrumental resolution as typical boundary thicknesses are on the order of a few nanometers. Composition is therefore averaged over an area that includes the grain boundary, some bulk material, and perhaps underlying grains. However, consistent variation between the average composition measured across a grain boundary and that measured for the grain for multiple analyses still yields useful information.

Total conductivity in air was performed on dense bars, approximately 3 mm × 4 mm × 14 mm using the a.c. impedance method in the direction of decreasing temperature. Minor electron−hole conductivity was separated from total electrical conductivity using the modified electromotive force (EMF) method first proposed by Gorelov.[20] This method increases measurement sensitivity and eliminates possible polarization errors in the determination of ion transference numbers; errors that are shown to be non-negligible for electrolyte-type materials which possess relatively minor electronic conductivity.[21] The experimental setup, measurement procedure, and comparison of this technique with the traditional approach are well-documented in the literature.[21] The activation energy (E_a) for the partial ionic conductivities was calculated by the standard Arrhenius equation

$$\sigma_o = \frac{A_o}{T}\exp\left[-\frac{E_a}{RT}\right] \quad (1)$$

where A_o is the pre-exponential factor.

Steady-state oxygen permeability was performed in a ceramic cell based on closed chambers with the material under study functioning as a permeating wall. An oxygen potential gradient is created between the inner and outer surfaces of the chamber walls by means of an electrochemical pump, as described elsewhere.[22,23] The absence of leaks was confirmed by monitoring the temperature dependence of permeability and the transient recovery of the cell from reducing to oxidizing conditions after current interruption, as described elsewhere.[24] Active membrane diameter was approximately 8 mm. All data on oxygen permeability presented in this article correspond to a membrane feed-side oxygen partial pressure (p_2) equal to atmospheric air (0.21 atm). The permeation processes are discussed using the quantities of oxygen flux density, j, and specific oxygen permeability, $J(O_2)$, which are interrelated as

$$J(O_2) = jd\left[\ln\frac{p_2}{p_1}\right]^{-1} \quad (2)$$

where p_1 is the oxygen partial pressure at the membrane permeate side ($p_1 < p_2$). As the quantity $J(O_2)$ is proportional to $j \times d$, by definition, the values of $J(O_2)$ should be thickness independent when surface limitations are negligible, eq 2. In this situation, $J(O_2)$ is proportional to the ambipolar conductivity (σ_{amb}), averaged for a given oxygen partial pressure range ($\overline{\sigma_{amb}}$), where t_o is the oxygen

(16) Fagg, D. P.; Shaula, A. L.; Kharton, V. V.; Frade, J. R. *J. Membr. Sci.* **2007**, *299*, 1.
(17) Fagg, D. P.; Kharton, V. V.; Frade, J. R. *J. Electroceram.* **2002**, *9*, 199.
(18) Fagg, D. P.; Abrantes, J. C. C.; Pérez-Coll, D.; Núñez, P.; Kharton, V. V.; Frade, J. R. *Electrochim. Acta* **2003**, *48*, 1023.
(19) Fagg, D. P.; Kharton, V. V.; Frade, J. R. *J. Solid State Electrochem.* **2004**, *8*, 618.
(20) Gorelov, V. P. *Elektrokhimiya* **1988**, *24*, 1380. [in Russian].
(21) Kharton, V. V.; Marques, F. M. B. *Solid State Ionics* **2001**, *140*, 381.
(22) Kharton, V. V.; Tikhnovich, V. N.; Shuangbao, L.; Naumovich, E. N.; Kovalevsky, A. V.; Viskup, A. P.; Bashmakov, L. A.; Yaremchenko, A. A. *J. Electrochem. Soc.* **1998**, *145*, 1363.
(23) Kharton, V. V.; Yaremchenko, A. A.; Valente, A. A.; Sobyanin, V. A.; Belyaev, V. D.; Semin, G. L.; Veniaminov, S. A.; Tsipis, E. V.; Shaula, A. L.; Frade, J. R. Rocha. *Solid State Ionics* **2005**, *176*, 781.
(24) Figueiredo, F. M.; Marques, F. M. B.; Frade, J. R. *Solid State Ionics* **1998**, *110*, 45.

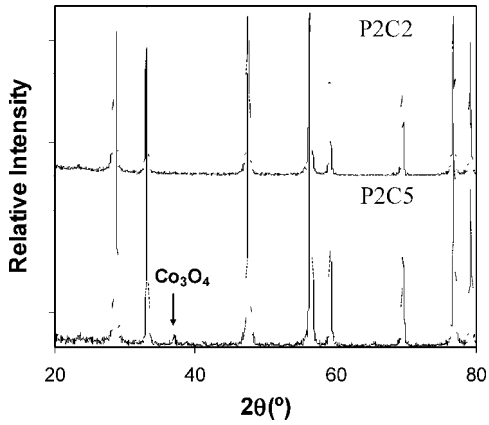

Figure 1. Expanded XRD patterns of P2C2 and P2C5 after sintering at 1000 °C for 5 h, to highlight a secondary phase of Co_3O_4 for composition P2C5, in addition to the cubic defect fluorite phase of $Ce_{0.8}Pr_{0.2}O_{2-\delta}$.

ion transference number and σ_T, σ_o, and σ_e represent the total, oxygen ionic, and electronic conductivities, respectively.

$$J(O_2) = \frac{RT}{16F^2}\overline{\sigma_{amb}} = \frac{RT}{16F^2}\frac{\sigma_o\sigma_e}{\sigma_o+\sigma_e} = \frac{RT}{16F^2}\overline{\sigma_T t_o(1-t_o)} \quad (3)$$

When oxygen surface exchange limitations are considerable the values of $J(O_2)$ should increase with membrane thickness due to a decreasing role of the surface exchange, for a given oxygen chemical potential gradient. The specific oxygen permeability therefore can be considered a useful tool with which to identify rate-limiting surface exchange effects on oxygen permeation, by analyzing its dependence on membrane thickness.[22]

For the EMF and permeability measurements a dwell time of 12 h was adopted before measurement at each temperature, leading to approximate total experimental times of 144 and 96 h, respectively. No degradation in performance was observed within the time scale of these experiments. All measurements were performed in the direction of decreasing temperature.

Data on oxygen stoichiometry was obtained by the coulometric titration technique. Coulometric titration were performed as a function of oxygen partial pressure at 950 °C in a double electrochemical cell in potentiostatic mode. Variations in oxygen content were measured with respect to a reference point of air, as described elsewhere.[25]

3. Results and Discussion

3.1. Structure, Sintering Behavior, and Thermal Expansion. Although all compositions exhibit the cubic defect fluorite structure by XRD, detailed inspection of the composition with 5 mol % Co additions (P25C), reveals the trace presence of Co_3O_4 (Figure 1). This is in contrast to the undoped composition (P2) and 2 mol % Co-doped composition (P2C2), which have previously been shown to be phase pure within the limits of resolution of XRD.[16] The lattice parameters presented in Table 1 are for materials normalized for thermal history, by sintering at 1000 °C for 5 h and then cooling to room temperature at 2 °C/min. Similar lattice parameters are exhibited by all samples, suggesting true solubilities of cobalt much lower than 2 mol %.

The shrinkage behavior of green compacts with a constant heating rate of 5 °C/min is compared in Figure 2. Sintering in the Co-free composition (P2) is incomplete at 1500 °C (the maximum temperature of the dilatometer used), while sintering in the Co-doped compositions has concluded at temperatures less than 1200 °C, Figure 2A. Parallels can be drawn with behavior observed in CGO materials,[17,18,26−29] where small additions of cobalt oxide were noted to be highly effective as sintering aids for the material $Ce_{0.8}Gd_{0.2}O_{2-\delta}$. The linear shrinkage rate $[d(\Delta L/L_0)/dT]$ when plotted as a function of temperature, Figure 2B, demonstrates that minor levels of Co-doping dramatically increase the maximum shrinkage rate and decrease the width of the shrinkage temperature range. For the compositions studied, the specific temperatures of maximum shrinkage rate are shown to be a function of Co content and to decrease with increasing Co content. Peak maxima are at 925 and 871 °C for the compositions 2 mol % Co-doped (P2C2) and 5 mol % Co-doped $Ce_{0.8}Pr_{0.2}O_{2-\delta}$ (P2C5), respectively. This assisted sintering allows pellets with densities greater than 90% that of the theoretical to be obtained under the processing conditions of 1000 °C for 5 h for the Co-doped samples in comparison to the requirement of 1600 °C for 10 h to achieve a similar density in the case of the Co-free sample.

The thermal expansion behavior of sintered materials is shown in Figure 3 to be similar for each composition, with a rapid increase in expansion at temperatures greater than 600 °C. Such irregular thermal expansion behavior has been shown in previous publications to be related to $Pr^{4+/3+}$ reduction.[5] The onset of this rapid increase in thermal expansion appears slightly delayed in the case of P2C5.

3.2. Microstructure. Figures 4 and 5 show TEM images of the compositions P2C2 and P2C5 respectively, densified at 1000 °C, whereas the microstructure of the Co-free composition sintered at 1600 °C can be found in refs 4, 5. The Co-containing compositions retain submicrometer grain sizes which are comparable for the two compositions. The much smaller grain sizes in the Co-containing compositions (Table 1) can be related to their lower sintering temperatures. The phenomena reported in the current article of assisted sintering, low temperature densification (∼1000 °C), and submicron grain size, agree with those reported for a wide range of transition metal oxide sintering aids for other ceria-based solid solutions. Despite this proliferance, the exact mechanism for the assisted sintering in these ceria-based solid solutions is still under debate.[17,18,26−32] Common to all reported cases is the detection of transition metal dopant enriched grain boundary regions by transmission electron

(25) Tikhonovich, V. N.; Zharkovskaya, O. M.; Naumovich, E. N.; Bashmakov, I. A.; Kharton, V. V.; Vecher, A. A. *Solid State Ionics* **2003**, *160*, 259.

(26) Jud, E.; Huwiler, C. B.; Gauckler, L. J. *J. Am. Ceram. Soc.* **2005**, *88*, 3013.

(27) Kleinlogel, C.; Gauckler, L. J. *SOFC-VI*; Singhal, S. C., Dokiya, M., Eds.; The Electrochemical Society: Pennington, NJ, 1999; Vol. 99-9, p 225.

(28) Kleinlogel, C.; Gauckler, L. J. *Solid State Ionics* **2000**, *135*, 567.

(29) Kleinlogel, C.; Gauckler, L. J. *Adv. Mater.* **2001**, *13*, 1081.

(30) Zhang, Z. L.; Wilfried, S. A.; Ruhle, M.; Jud, E.; Gauckler, L. J. *Acta Materialia* **2007**, *55*, 2907.

(31) Lewis, G. S.; Atkinson, A.; Steele, B. C. H. *4th European Solid Oxide Fuel Cell Forum*; Bossel, U., Ed.; Oberrohrdorf, Switzerland, 2000; p 733.

(32) Jud, E.; Zhang, Z.; Sigle, W.; Gauckler, L. J. *J. Electroceram.* **2006**, *16*, 191.

Table 1. Average Grain Size, Lattice Parameters and Apparent Activation Energies for the Partial Ionic Conductivity and Oxygen Permeability of $Ce_{0.8}Pr_{0.2}O_2$-Based Materials Prepared in Air

			ionic conduction[a]		oxygen permeation [b]	
composition	avg grain size (μm)	lattice param (Å), ± 0.002 Å	E_a(kJ mol^{-1})	temperature range (°C)	E_a(kJ mol^{-1})	temperature range (°C)
P2	3.5 ± 0.5	5.4100	57 ± 2	950−800	98 ± 7	1000−800
P2C2	0.14 ± 0.02	5.4106	56 ± 3	950−800	54 ± 6	850−750
P2C5	0.16 ± 0.07	5.4083	84 ± 3	950−800	77 ± 11	850−750

[a] Air/oxygen gradient. [b] Log(p_2/p_1) = 1, membrane thickness 1 mm.

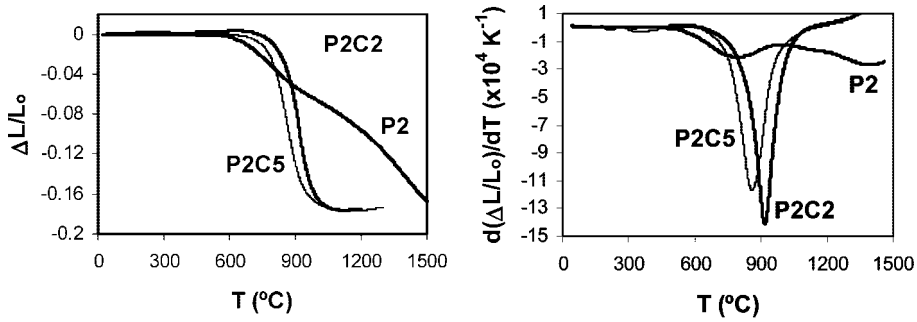

Figure 2. Influence of 2 mol % (P2C2) and 5 mol % (P2C5) additions of cobalt oxide to $Ce_{0.8}Pr_{0.2}O_{2-\delta}$ (P2) on the temperature dependence of the linear shrinkage (A) and the linear shrinkage rate (B).

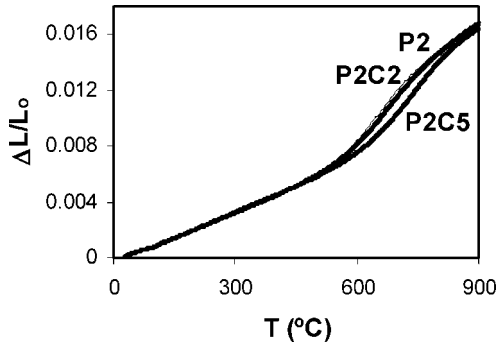

Figure 3. Linear thermal expansion behavior of dense compositions P2, P2C2, and P2C5 in air.

microscopy/ energy dispersive analysis TEM/EDS or electron energy loss spectrometry (EELS). For this reason a careful study of the grain boundary regions by TEM is essential to the understanding of these materials. The interface between grains for the P2C2 composition is very fine, appearing almost continuous (see images B and C in Figure 4), whereas in the case of P2C5, the grain boundary region appears more defined, Figure 5B. Furthermore, in the case of P2C5, distinct fringes can often be located as shown in Figure 5C.

EDS analysis, Figure 6, shows that the additive is preferentially sited in the grain boundary region, in agreement with previous studies on Co-doped CGO.[17,18,26,29−32] This result suggests a very low solubility of Co in these materials, in agreement with that noted for pure ceria[33] and also for the comparable material $Ce_{0.9}Gd_{0.1}O_{2-\delta}$ where solubilities of approximately 0.5 mol % at 900 °C have been estimated.[34,35] In the case of P2C5, the composition of the fringes is similar to that of the grain boundary, with both regions exhibiting the presence of Co, Figure 6B. In conclusion, the concentration of 5 mol % Co additive appears to be too great to be well distributed in the grain boundary regions. Instead, one can observe less fine grain interfaces and segregated zones that contain Co. This result coincides well with the appearance of Co_3O_4 as a secondary phase in the XRD result for this composition (Figure 1).

3.3. Electrical Characterization. At the highest temperatures, the presence of Co leads to a slight enhancement in total conductivity in air when compared to the Co-free composition P2 (Figure 7A). Although this advantage is maintained to lower temperatures in the case of P2C2, the total conductivity of CP25 is shown to rapidly decrease to match the level of conductivity in composition P2 by approximately 700 °C. Figure 7B, presents the temperature dependence of the oxygen ion transference numbers, obtained by the modified EMF method, across a $p(O_2)$ gradient of 1.0/0.21 atm (oxygen/air) for the three samples. As mentioned in the Experimental Section, these measurements are made during extended periods of time at temperatures above 700 °C, where oxygen exchange with the atmosphere would be thought to be in equilibrium, with no observable degradation of properties during the time scale of the experiments.[16−18] Both 2 and 5 mol % Co-additions promote substantially lower ionic transference numbers than that obtained in the parent composition P2. The positive temperature dependencies of ionic transference numbers for P2 and P2C2 are comparable, whereas the composition P2C5 exhibits much stronger temperature dependence. Figure 7C shows the temperature dependence of the ionic conductivities measured in the $p(O_2)$ gradient 1.0/0.21 atm calculated by the combination of transference numbers with the total conductivity values obtained by impedance spectroscopy at corresponding temperatures.

$$\sigma_o = t_o \sigma_T \quad (4)$$

The level of ionic conductivity is comparable for both the compositions P2 and P2C2 and with similar activation

(33) Chen, M.; Hallstedt, B.; Grundy, A. N.; Gauckler, L. J. *J. Am. Ceram. Soc.* **2003**, *86*, 1567.
(34) Jud, E.; Gauckler, L. J. *J. Electroceram.* **2005**, *15*, 159.
(35) Sirman, J. D.; Waller, D. AndKilner, J. A. *SOFC-V*; Stimming, U., Singhal, S. C., Tagawa, H., Lehnert, W. A., Eds.; The Electrochemical Society: Pennington, NJ, 1997; p 1159.

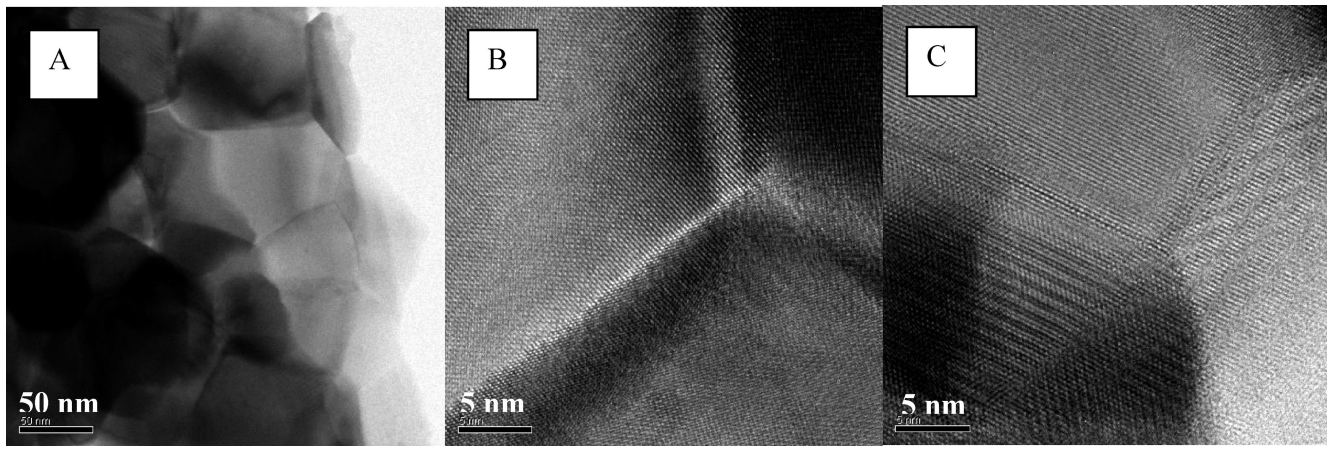

Figure 4. Transmission electron microscopy images of $Ce_{0.8}Pr_{0.2}O_{2-\delta}$ containing 2 mol % cobalt oxide additions sintered at 1000 °C for 5 h.

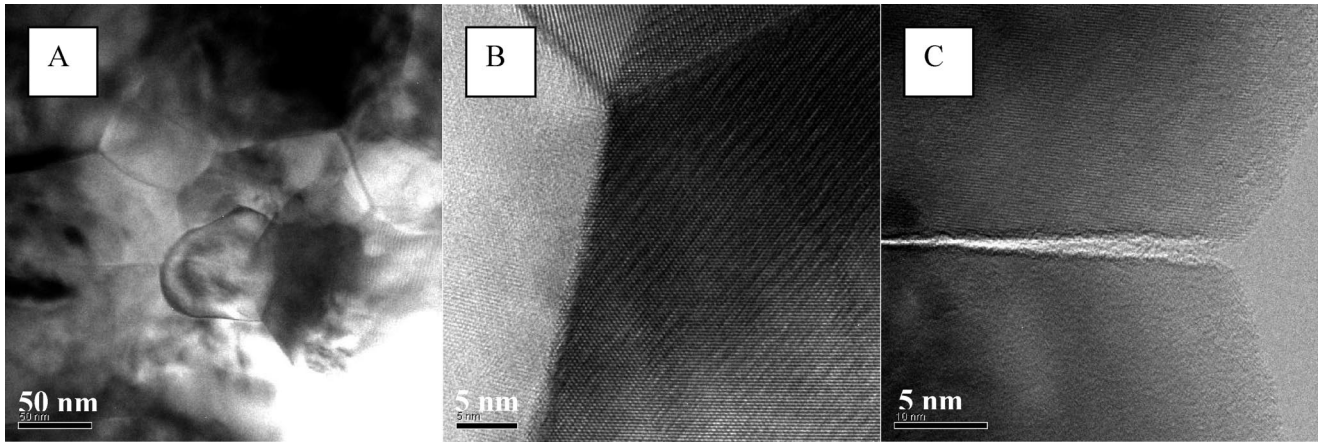

Figure 5. Transmission electron microscopy images of $Ce_{0.8}Pr_{0.2}O_{2-\delta}$ containing 5 mol % cobalt oxide additions sintered at 1000 °C for 5 h.

energies (Table 1). In stark contrast, the ionic conductivity of composition P2C5 exhibits greater activation energy, causing ionic conductivities that are depleted in comparison to the other compositions at lower temperatures. Therefore, one can state that the presence of 2 mol % cobalt oxide does not affect the level or the nature of the ionic conductivity in these materials, while a greater concentration of cobalt oxide is detrimental. Figure 7D presents the electronic conductivities estimated from the equation

$$\sigma_e = (1 - t_o)\sigma_T \quad (5)$$

The presence of cobalt oxide as a sintering additive leads to an enhancement in electronic conductivity in compositions P2C2 and P2C5 of approximately 2−3 times with respect to the Co-free composition, $Ce_{0.8}Pr_{0.2}O_{2-\delta}$. The magnitude of this enhancement is very slightly higher in the P2C5 case. The nonlinear temperature dependence of the electronic conductivity of P2 is due to reduction of Pr^{4+} to Pr^{3+} at elevated temperatures and subsequent temperature dependence of the number of electronic charge carriers.[5,36] It is interesting that such extreme behavior is not observed in P2C2 and P2C5. This factor will be discussed later.

The enhancement of electronic conductivity by minor additions of cobalt oxide is a comparable phenomenon to that observed in the well studied electrolyte material $Ce_{0.8}Gd_{0.2}O_{2-\delta}$ (CGO) in which minor, 2 mol%, additions of transition metal (e.g., Cu,Co,Fe) sintering aids can produce enhancements of p-type conductivities of up to 25 times.[17,18] In the case of CGO, the source of these elevated electronic conductivities has been suggested to be the incomplete incorporation of the transition metal additive in the bulk, and the preferential formation of transition element rich grain boundary layers. Furthermore, because of the fact that the sintering additives lead to smaller grain sizes and an increase in effective grain boundary length, previous authors have suggested that the grain boundary layers in these materials should be electronically conductive and that the presence of the variable valence transition metal additives must produce a percolating network for electronic transport.[17,32,34,37] The recorded microstructures for the current materials support this hypothesis as similar grain boundary locations for the Co additive have been observed. However, one should be cautious to definitively state for the current materials that the increased electronic conductivity arises because of conductive grain boundary networks; the grain bulk is also mixed conducting because of small polaronic hopping between Pr^{4+} and Pr^{3+} ions.[5] One must, therefore, eliminate the possibility that the Co additions are influencing the Pr

(36) Zhou, G.; Gorte, R. J. *J. Phys. Chem. B* **2008**, *112*, 9869.

(37) Pérez-Coll, D.; Núñez, P.; Abrantes, J. C. C.; Fagg, D. P.; Kharton, V. V.; Frade, J. R. *Solid State Ionics* **2005**, *176*, 2799.

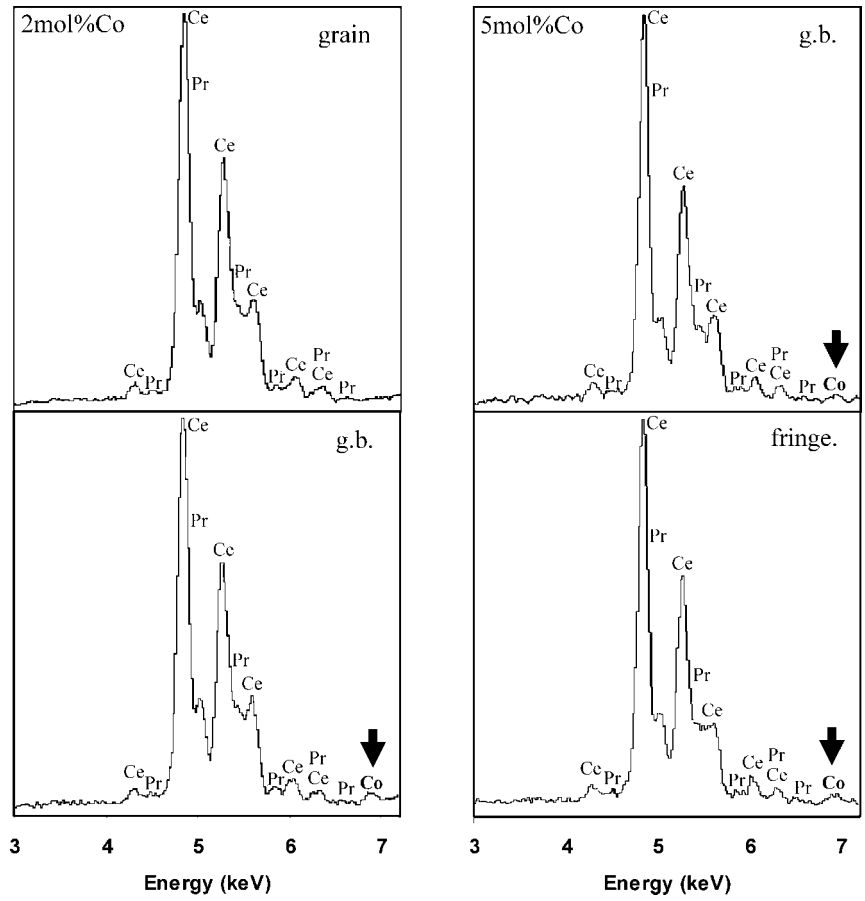

Figure 6. XEDS analysis of compositions P2C2 and P2C5, showing a grain boundary location of the sintering additive. Co-containing fringes are observed in the case of composition P2C5.

oxidation state as this phenomenon would also alter the level of measured electronic conductivity.[5] To fulfill this prerequisite, we have performed coulometric titration measurements as described in the following section.

3.4. Coulometric Titration. Further information on the location of the additive can be taken from the expected defect chemisty. The base material $Ce_{0.8}Pr_{0.2}O_{2-\delta}$ contains two cations, Pr and Ce, which have the capacity to exhibit mixed valency. However, as described in the literature,[5] the dominant defect equilibrium at higher oxygen partial pressures, can be considered to be that of Pr reduction. Hence, for the current experimental conditions, one can assume that mixed conduction in the bulk will arise because Pr reduction, given by the equation

$$2Pr_{Ce}^{x} + O_{O}^{x} \overset{K}{\leftrightarrow} 2Pr_{Ce}^{/} + V_{O}^{\bullet\bullet} + \frac{1}{2}O_2 \qquad (6)$$

However, in the current materials, we also add small concentrations of variable valent cobalt ions as sintering additives. One can, therefore, imagine two distinct scenarios. The first is that the additive is completely insoluble in the bulk and as such has no influence on the bulk defect chemistry, whereas the second is that some solubility of the Co additive would occur in the bulk and be charge compensated either by an increase in bulk vacancy concentration or alternatively by an increase in the average Pr oxidation state. Clearly, the results of the microstructural examination strengthen the first hypothesis, that the Co-additives are relatively insoluble in the bulk material and are preferentially located in the grain interfaces. However, to be able to state implicitly that the elevated electronic conductivity is due to the presence of Co in the grain boundary regions, and not due to some additional influence of the additive on Pr oxidation state,[5] it is necessary to envisage a test condition under which the cobalt oxide would retain a constant oxidation state, and where it may be simply introduced into the defect chemistry.

The reduction temperature of Co_3O_4 to CoO has been documented to occur at 935 °C when present as a sintering additive in CGO.[34] For this reason, coulometric titration studies are performed at 950 °C; a temperature at which the Co oxidation state can be considered constant, as all cobalt will be present as Co^{2+}.[38] Under these conditions, one can write the following defect relations for the two extremes of Co additive location; first (model A), all additive is located in the grain boundaries, or second (model B), all additive is accommodated into the bulk.

(i) Grain Boundary location of additive (model A). In this scenario, the additive does not influence the bulk defect chemistry. The defect relations of the bulk can therefore be written as in ref 5. Following the typical Brouwer approach,[39] the electroneutrality relation under these higher oxygen partial pressures can be simplified as

(38) Chen, M.; Hallstedt, B.; Gauckler, L. J. *J. Phase Equilib.* **2003**, *24*, 212.
(39) Brouwer, G. *Philips Res. Rep.* **1954**, *9*, 366.

$$[Pr'_{Ce}] = 2[V_O^{\bullet\bullet}] \text{ as } [Pr'_{Ce}] \gg [Ce'_{Ce}] \text{ at high } pO_2 \quad (7)$$

For the composition $Ce_{0.8}Pr_{0.2}O_{2-\delta}$, one can write the relationships

$$[O_O^x] = 2 - \alpha \quad (8)$$

$$[V_O^{\bullet\bullet}] = \alpha \quad (9)$$

and using the electroneutrality relation, eq 7

$$[Pr_{Ce}^x] = 0.2 - 2\alpha \quad (10)$$

$$[Pr'_{Ce}] = 2\alpha \quad (11)$$

the relationship describing the equilibrium constant of Pr reduction, eq 6, therefore can be written as

$$K = \frac{4\alpha^2 pO_2^{1/2}}{(0.2 - 2\alpha)^2(2 - \alpha)} \quad (12)$$

In a similar way, we can now discuss the defect chemistry of the alternative location of the sintering additive in the grain bulk.

(ii) Bulk location of additive (model B). The accommodation of the Co^{2+} in the grain bulk can be expressed by the following substitution mechanism, where x is the fraction of Co accommodated.

$$(1-x)Ce_{0.8}Pr_{0.2}O_{2-\alpha} + xCoO \rightarrow Ce_{(0.8-0.8x)}Pr_{(0.2-0.2x)}Co_xO_{2-x-\alpha} \quad (13)$$

Using the Brouwer approach,[39] at more oxidizing conditions and for temperatures above the reduction temperature of Co_3O_4, the electroneutrality relation, can be written as

$$[Pr'_{Ce}] + 2[Co''_{Ce}] = 2[V_O^{\bullet\bullet}]$$

leading to the relationships

$$[Co''_{Ce}] = x \quad (14)$$

$$[O_O^x] = 2 - x - \alpha \quad (15)$$

$$[V_O^{\bullet\bullet}] = x + \alpha \quad (16)$$

$$[Pr_{Ce}^x] = 0.2 - 0.2x - 2\alpha \quad (17)$$

$$[Pr'_{Ce}] = 2\alpha \quad (18)$$

leading to the following expression for the equilibrium constant of Pr reduction, eq 6

$$K = \frac{4\alpha^2(\alpha + x)pO_2^{1/2}}{(0.2 - 0.2x - 2\alpha)^2(2 - x - \alpha)} \quad (19)$$

The coulometric titration results for compositions P2 and P2C2 at 950 °C are presented in Figure 8A in the form of $pO_2 - T - \Delta\delta$ diagrams for the oxygen partial pressure range 1×10^{-4} to 0.21 atm, with respect to a reference point of air. Note that no additional information would be offered by testing P2C5 as the solid solubility of Co is plainly exceeded in this composition due to the presence of Co_3O_4 shown by XRD, Figure 1. The following relationship can be deduced, which is valid for both locations of the sintering additive, model A and model B.

$$\Delta\delta = [V_O^{\bullet\bullet}] - [V_O^{\bullet\bullet}]^{air} = \Delta\alpha \quad (20)$$

In these more oxidizing conditions, an increase in oxygen nonstoichiometry is observed with decreasing oxygen partial

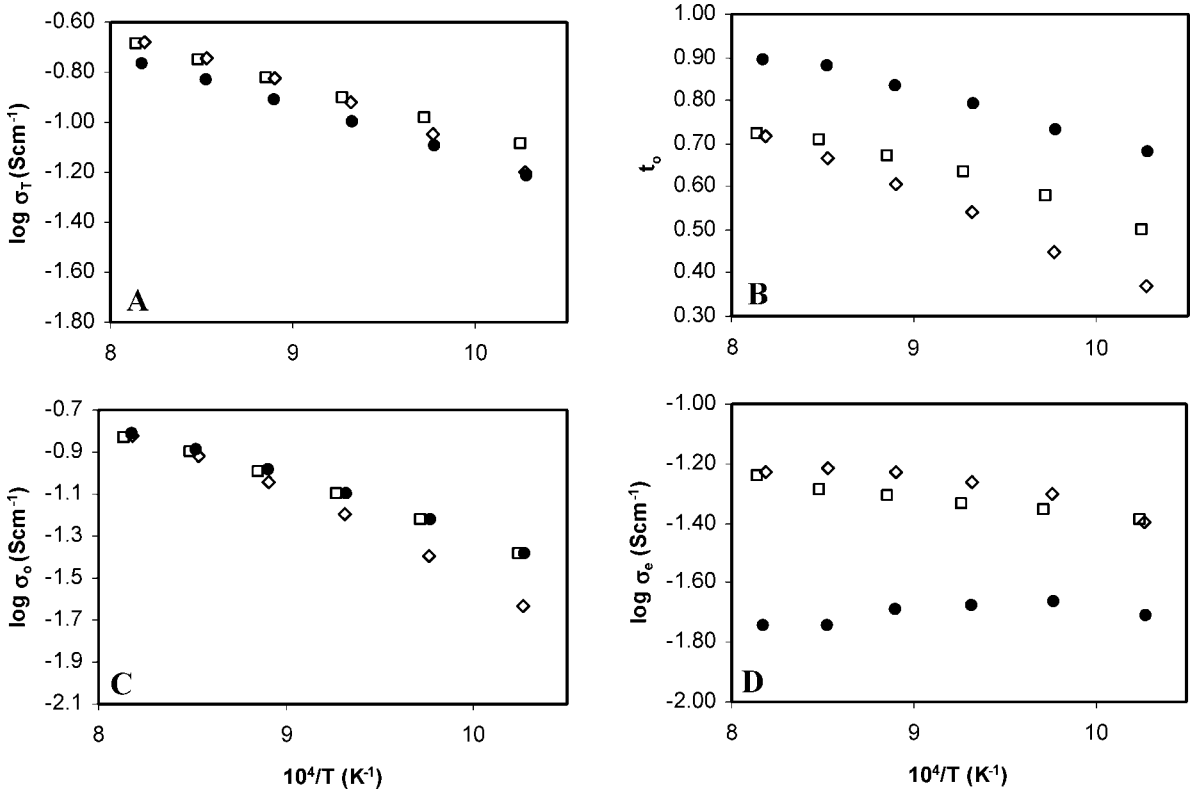

Figure 7. Influence of 2 and 5 mol % additions of cobalt oxide on the temperature dependence of (A) total conductivity, (B) ionic transference number, (C) ionic conductivity, and (D) electronic conductivity of $Ce_{0.8}Pr_{0.2}O_{2-\delta}$, in the oxygen partial pressure gradient, 1.0/0.21 atm. Open squares, P2C2; filled circles, P2; open diamonds, P2C5.

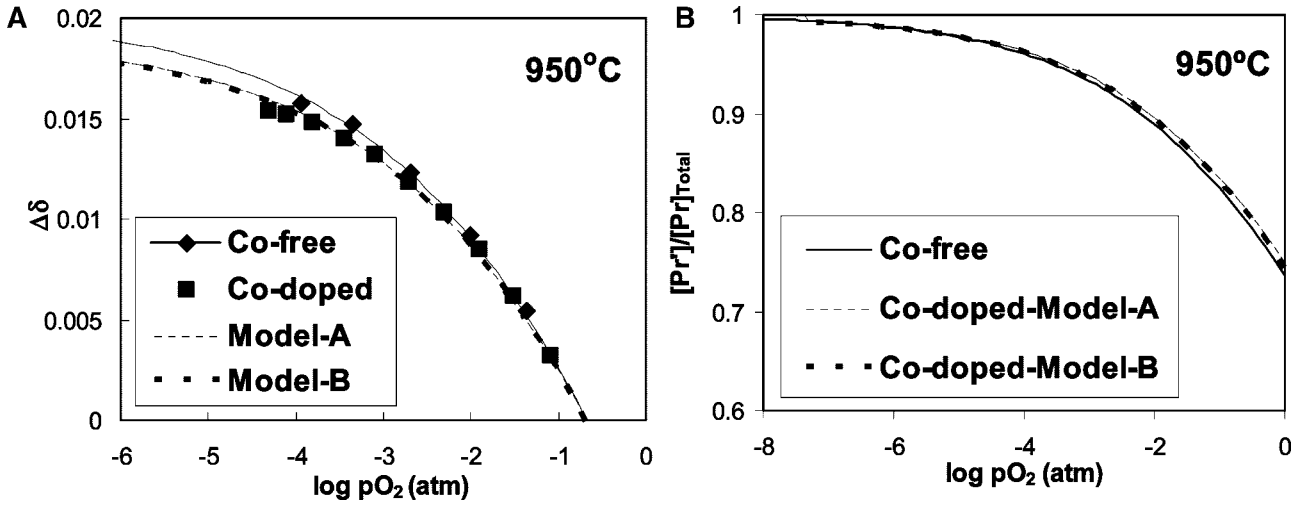

Figure 8. (A) Oxygen partial pressure dependence of oxygen nonstoichiometry and (B) the calculated fractional concentration of Pr in the 3+ oxidation state with respect to a reference point of air in the system $Ce_{0.8}Pr_{0.2}O_{2-\delta}$ at 950 °C, compared to that calculated for composition P2C2 for a bulk or a grain boundary location of the additive. Lines represent fits to experimental data (symbols) constrained by eqs 12 or 19.

pressure. Respective values of the equilibrium constant, K, can subsequently be determined for each specific case, which best describe the experimental dependence of sample oxygen nonstoichiometry on pO_2, constrained by eqs 12 and 19. The best fit values of K are summarized in Table 1, whereas the fit to the experimental data described by eqs 12 and 19 is represented by lines through the data points in Figure 8 (A) and compared with results for P2 taken from ref. 5. The fractional concentration of Pr in the 3+ oxidation state can be calculated in model A, from eqs 10 and 11, as

$$\frac{[Pr'_{Ce}]}{[Pr_{Ce}]_{Total}} = 10\alpha \tag{21}$$

and in model B, from eqs 17 and 18, as

$$\frac{[Pr'_{Ce}]}{[Pr_{Ce}]} = \frac{10\alpha}{1-x} \tag{22}$$

Figure 8B represents the pO_2 dependence of the fractional concentration of Pr in the 3+ oxidation state calculated for the values of equilibrium constant K, for the two Co-containing models for composition P2C2 given in Table 1 and compared to results for composition P2 taken from ref 5. One observes that the fractional concentration of Pr^{3+} is similar for all models, and complete reduction of Pr is predicted by approximately 1×10^{-8} atm.

If the Co addition were accommodated into the bulk material and charge compensated by an increase in the oxidation state of Pr, one would expect a decrease in the fractional concentration of Pr3+ between compositions P2 and P2C2. The observed results, therefore, do not agree with this hypothesis. On the contrary, the fractional concentration of Pr^{3+} is virtually unchanged between the experimental results of Co-containing and Co-free compositions and can be considered to be equal within experimental error. Furthermore, the reducibility of Pr seems to be unaffected by the presence of Co, with a similar dependence on pO_2 noted for the two compositions. From these results, one can draw the definitive conclusion that the Co additive is not charge compensated by modifications of the Pr oxidation state.

3.5. Discussion of the Electrical Properties. The coulometric titration experiments conclude that the Co additives do not influence the Pr oxidation state. The other option for bulk accommodation of the additive is that charge compensation may occur by an increase in oxygen vacancy concentration. Comparison of the vacancy concentration required for this charge compensation mechanism for P2 and P2C2, can be made by equating eqs. 21 and 22 and substituting eqs. 9 and 16

$$[V_O^{\bullet\bullet}]_{P2}(1-x) + x = [V_O^{\bullet\bullet}]_{P2C2} \tag{23}$$

The increase in vacancy concentration described by eq 23 for this charge compensation mechanism is at a level that would have significant consequence on the level of ionic conductivity. For both the current base material $Ce_{0.8}Pr_{0.2}O_{2-\delta}$[4-6] and for related doped ceria materials with similar high dopant contents, a rapid decrease in ionic conductivity with increasing vacancy concentration is a characteristic phenomenon, which is related to microdomains of ordering.[40] However, in contrast to such prediction of a depleted ionic conductivity with increasing vacancy concentration, the ionic conductivity of composition P2C2 and P2 are shown to be virtual equal, Figure 7C. For this reason, one can suggest that this charge compensation mechanism for Co additions is also highly unlikely, and further supports the argument that the Co additive is not soluble in the grain bulk.

The defect chemistry of the base composition $Ce_{0.8}Pr_{0.2}O_{2-\delta}$ is documented in the literature.[5] The electronic conductivity of this composition in oxidizing conditions was suggested to be controlled by small polaronic hopping between Pr ions of different valency, limited by the number of available sites for electron hops, described as

$$\sigma_e = K[Pr'_{Ce}]([Pr_{Ce}]_{Total} - [Pr'_{Ce}]) \tag{23a}$$

The EMF study reported that the Co-containing composition P2C2 exhibits an enhancement of electronic conductivity of

(40) Kilner, J. A.; Steele, B. C. H. *Non-Stoichiometric Oxides*; Sørensen, O., Ed.; Academic Press: New York, 1981; p 233.

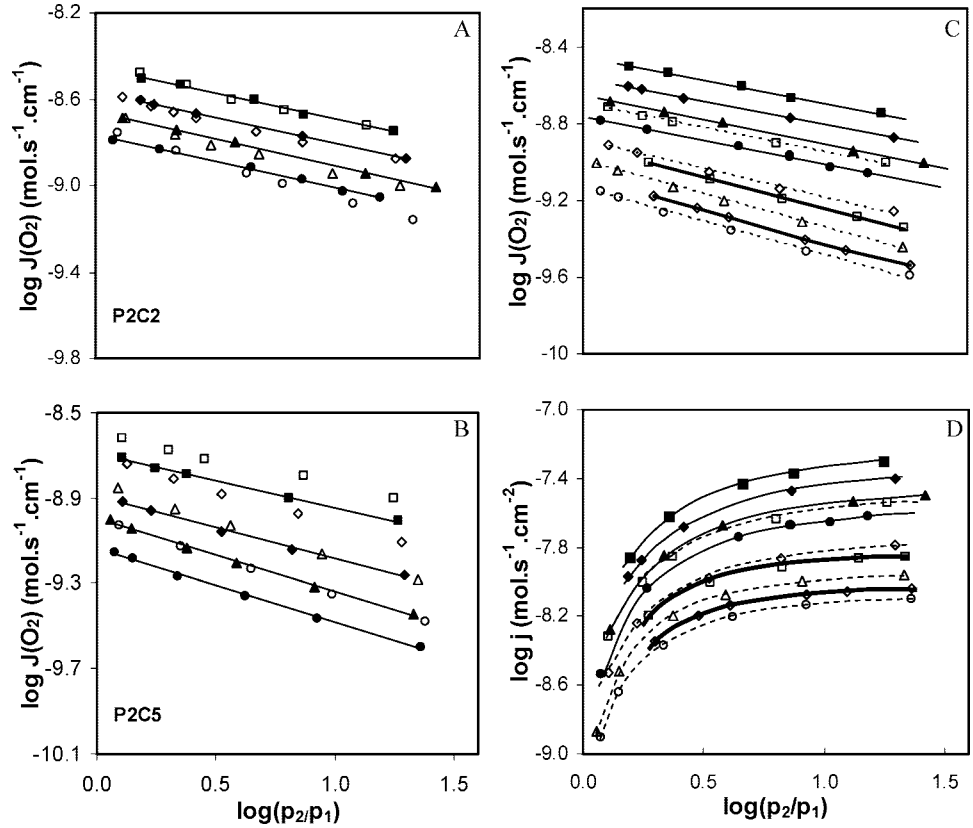

Figure 9. (A, B) Oxygen chemical potential gradient dependencies of the specific oxygen permeability through membranes of different thicknesses of (A) P2C2 and (B) P2C5, highlighting the presence of surface limitations in the case of P2C5. P2C2 open symbols 1.4 mm, closed symbols 1 mm, P2C5 open symbols 1.3 mm, closed symbols 1 mm. (C, D) Oxygen chemical potential gradient dependencies of the (C) steady state oxygen permeation flux and the (D) corresponding specific oxygen permeability $Ce_{0.8}Pr_{0.2}O_{2-\delta}$ membranes with identical membrane thicknesses (1 mm). Thick line, P2; thin line, P2C2; dashed line, P2C5. Squares, 850 °C; diamonds, 800 °C; triangles, 750 °C; circles, 700 °C.

about 2−3 times over the base composition P2 in oxidizing conditions, Figure 7D. To achieve this level of enhancement of electronic conductivity from solely a change in the fractional concentration of Pr^{3+}, eq. 23 would predict a substantial decrease in the concentration of Pr^{3+} because the Pr^{3+}/Pr^{4+} ratio in P2 is already beyond that of the conductivity maxima. This clearly does not concur with the results of the coulometric titration experiments, which conclude that the Pr oxidation state is basically unaffected by the Co additions. For this reason, one can unequivocally state that the enhancement in electronic conductivity on addition of cobalt oxide to $Ce_{0.8}Pr_{0.2}O_{2-\delta}$ is not related to changes in the Pr oxidation state in the bulk material but instead must arise due to conductive grain boundary networks rich in the additive, in agreement to that suggested in the literature for the similar material CGO,[17,32,34,37] and to that suggested by the microstructural examination. Supplementary evidence in support of this suggestion is given by the more linear temperature dependences for electronic conduction in the Co-containing compositions in comparison to that noted in P2, Figure 7D.

In summary, Coulombic titration has shown the bulk defect chemistry to be unaffected by the Co-addition. This result coupled with the measured ionic and electronic conductivities can reinforce the microstructural observations to unequivocally state that the Co additions are highly insoluble in the bulk material and instead form electronically conducting grain boundary networks rich in the additive. These additives lead to an enhanced electronic conductivity of about 2−3 times, whereas low concentrations of these additives do not adversely impact ionic conductivity. Higher concentrations of additive, however, lead to a depleted ionic conductivity. As a low solubility of the additive in the bulk material is proven, the depleted ionic conductivity at higher concentration must be due to the intergranular prevention of ionic motion, a hypothesis which is supported by the observation of more distinct grain boundary regions and fringes in the microstrutural examination of the composition P2C5.

3.6. Oxygen Permeability. The specific oxygen permeability, $J(O_2)$, measured through different membrane thicknesses of the Co-doped materials, is presented in Figure 9 as a function of oxygen partial pressure gradient. As highlighted in the experimental section this test is a useful tool with which to identify rate-limiting surface exchange effects on oxygen permeation. Figure 9A confirms the absence of oxygen surface exchange limitations for composition P2C2, as the values of specific oxygen permeability are equal for the two thicknesses within the confines of experimental error.[16] In contrast, oxygen surface exchange limitations are documented for the composition, P2,[4,6] and are now confirmed to be present for composition P2C5 in Figure 9B, by the characteristic result of a lower specific oxygen permeability with decreasing membrane thickness.[22] The presence of 2 mol % cobalt oxide, therefore, can significantly improve oxygen surface exchange in comparison to the base composition P2, whereas this benefit is observed to be impaired at a higher Co-content.

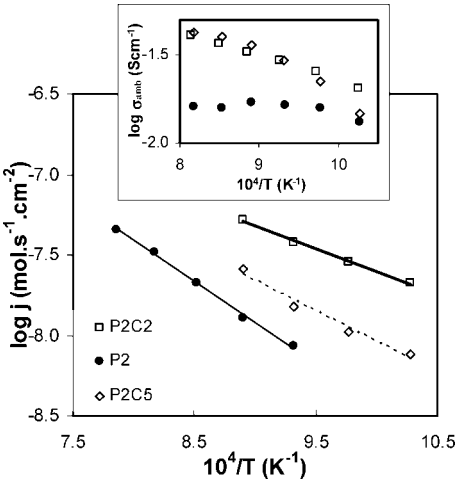

Figure 10. Influence of additives on the temperature dependence of the oxygen permeation flux of $Ce_{0.8}Pr_{0.2}O_{2-\delta}$ under identical membrane thicknesses and oxygen partial pressure gradients, $\log(p_2/p_1) = 1$, membrane thickness 1 mm. Insert shows the temperature dependence of ambipolar conductivity calculated from results of the E.M.F measurements in Figure 7.

The addition of 2 mol % cobalt oxide to the comparable material CGO is documented to cause dramatic improvements in oxygen reduction kinetics due to an increased electronic conductivity and a grain boundary network rich in cobalt oxide.[17] The current materials P2C2 and P2C5 both show grain boundary locations of Co additive and similar enhanced levels of electronic conductivities in comparison to that of the base material P2. Because of this similarity, it is perhaps surprising that both compositions do not exhibit comparable improvements in oxygen surface exchange. On the contrary, the amount of additive appears to be a critical factor that radically impacts surface exchange. One possible explanation can be suggested from the microstructures of P2C2 and P2C5. Composition P2C5 possesses a microstructure with pronounced grain boundary layers and Co-rich fringes, features that may conceivably block ionic transport and prevent the substantial enhancement in oxygen surface exchange offered by the more continuous intergrain structure observed in the case of P2C2. The presence of these microstructural features was suggested to be the cause of the depleted ionic transport measured for P2C5 in Figure 7C. The permeation results appear to further this line of discussion, provoking the hypothesis that these microstructural features may also hinder oxygen exchange at the sample surface.

The Co-containing compositions exhibit an enhanced specific oxygen permeability Figure 9C and corresponding steady state oxygen permeation flux Figure 9D when compared to the Co-free composition P2, for identical membrane thicknesses, and this enhancement is largest in the case of composition P2C2.

The temperature dependence of oxygen permeation flux increases in the order P2C2 < P2C5 < P2, Figure 10; corresponding activation energies are listed in Table 1. This variation in temperature dependence and the much higher steady-state permeation flux measured for the composition P2C2 cannot be explained solely by the enhancement ambipolar conductivity in the Co-containing compositions

Table 2. Fitting Parameters for $Ce_{0.8}Pr_{0.2}O_{2-\delta}$ (P2), with 2 mol % Co Additions (P2C2), for the Two Extreme Cases of Co Location: (Model A) Insoluble and Present in the Grain Boundary or (Model B) Soluble in the Grain Bulk

composition	K ± 0.005 (atm$^{0.5}$)	
P2	0.300	
P2C2	model A g.b. 0.350	model B grain 0.415

reported in the inset of Figure 10. Indeed, the ambipolar conductivities of compositions P2C2 and P2C5 appear to be very similar at temperatures above 750 °C and have activation energies that far exceed that of composition P2. Instead, the absolute values and the temperature dependences of oxygen permeation flux originate from the combination of improved ambipolar conductivities combined with reduced oxygen surface exchange limitations in the Co-doped cases. In the case of P2C2, the kinetics of surface exchange are high enough to not limit oxygen permeation, Figure 9A, leading to a much higher permeation flux than that obtainable in a material of similar ambipolar conductivity, P2C5, which suffers oxygen surface exchange limitations, Figure 9B. The resultant small activation energy for oxygen permeability exhibited by the 2 mol % Co-doped $Ce_{0.8}Pr_{0.2}O_{2-\delta}$ material (54 kJ mol^{-1}) allows it to offer levels of oxygen permeation flux at temperatures below 850 °C that can compete with some of the more common perovskite membranes suggested for high oxygen permeability in the literature.[1,2,16]

4. Conclusions

The introduction of minor additions of cobalt oxide are highly effective as a sintering additive in the fluorite-type material $Ce_{0.8}Pr_{0.2}O_{2-\delta}$ allowing dense materials to be formed at 1000 °C with submicrometer-sized grains. X-ray energy dispersive spectroscopy shows that the additive is located in the grain boundary. Fine grain interfaces are obtained for 2 mol % Co additions, whereas more pronounced grain boundary layers and Co-rich fringes are noted at the higher cobalt oxide content of 5 mol %.

The additions of cobalt oxide lead to a slightly enhanced total conductivity due to an enhanced electronic conductivity of around 2−3 times. For 2 mol % additions of sintering additive, no change to the level or nature of ionic conductivity is observed, whereas at 5 mol %, a depleted ionic conductivity is noted at lower temperatures. The bulk Pr oxidation state is shown to be unaffected by the cobalt oxide additions, when analyzed by Coulombic titration. The combination of this result with the observed electrical properties reinforces the microstructural analysis to unequivocally state that the Co additions are not accommodated in the bulk material but form grain boundary networks rich in the additive. These grain boundary networks are conductive and lead to the observed enhancement in electronic conduction.

Co additions produce a decrease in ionic transference number and an increase in the ambipolar conductivity. Of paramount importance, the presence of cobalt oxide also leads to substantial improvements in the kinetics of oxygen surface exchange. At the concentration of 2 mol % sintering additive, materials free from oxygen surface exchange limitations can be produced, whereas at 5 mol % additions

this benefit is impaired. This is suggested to be related to the presence of more pronounced grain boundary layers and Co-rich fringes at higher Co contents, which may block ionic transport and cause surface exchange limitations.

Hence, the combination of an enhanced ambipolar conductivity and enhanced of oxygen surface exchange kinetics boosts the level of oxygen permeability in 2 mol % cobalt oxide doped $Ce_{0.8}Pr_{0.2}O_{2-\delta}$, to levels that can compete with some of the best perovskite-type oxygen permeation membranes at temperatures below 850 °C, and also produces one of the highest levels of oxygen permeability reported to date for a stable, single-component, mixed-conducting, fluorite material.

Acknowledgment. This work was supported by the FCT, Portugal (projects PTDC/CTM/66243/2006, SFRH/BPD/3529/2000, and REEQ/710/CTM/2005). S.G.-M, thanks the Spanish MEC for funding Project MAT2007-64486-C07-04 and CAM for Project MATERYENER S 505/PPQ/0358. The authors also thank the Microscopy Centre Luis Bru from UCM for technical assistance.

CM802708A